Kinetic Investigation of η-Al₂O₃ Catalyst for Dimethyl Ether Production

Ahmed I. Osman[1,2] · Jehad K. Abu-Dahrieh[1]

Abstract

Herein, kinetic modelling and kinetic parameters were used to study methanol dehydration to dimethyl ether reaction and revealed that the best model to fit the experimental data was the Bercic model. The dehydration reaction undergoes dissociative adsorption Langmuir–Hinshelwood mechanism of methanol on the alumina catalyst surface, with the calculated value of the activation energy was 136.7 kJ mol^{-1}. Moreover, the effect of different kinetic parameters such as the catalyst weight and methanol concentration or water in the feed on the catalytic performance of η-Al₂O₃ was examined in a fixed bed reactor under the reaction conditions where the temperature ranged from 180 to 350 °C with a WHSV = 12.1 h^{-1}.

Graphical Abstract
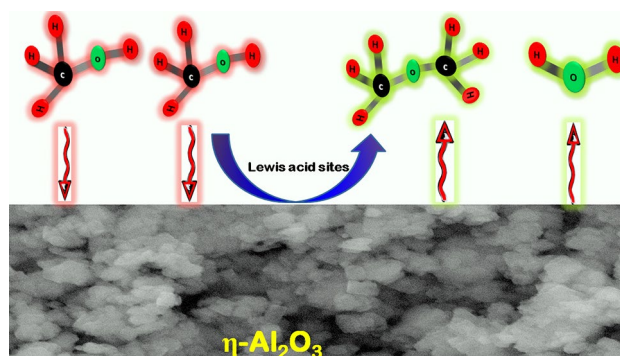
✉ Ahmed I. Osman
aosmanahmed01@qub.ac.uk

✉ Jehad K. Abu-Dahrieh
j.abudahrieh@qub.ac.uk

1 School of Chemistry and Chemical Engineering, Queen's University Belfast, David Keir Building, Stranmillis Road, Belfast BT9 5AG, Northern Ireland, UK

2 Chemistry Department, Faculty of Science - Qena, South Valley University, Qena 83523, Egypt

1 Introduction

Energy consumption throughout the world has been continuously increased especially for industrialized cities. The carbon-based non-renewable sources, mainly crude oil, are unsustainable because of the production of the significant amount of greenhouse gases in which is the main cause of the global warming. To meet the energy demand and decrease the air pollution an alternative renewable energy should be developed. The production of clean biofuel such as dimethyl ether (DME) is an attractive alternative for pollution mitigation. DME is an environmentally friendly fuel with clean-burning and smoke-free emissions [1]. The attractive combustion properties are due to it containing neither sulphur nor nitrogen, with very low SO$_x$ or NO$_x$ emissions. The lack of direct carbon-to-carbon bonds means it

does not generate particulate matter emissions. DME can be produced by two main routes; either from syngas using a bi-functional catalyst (Eq. 1) or via the dehydration of methanol over solid catalysts such as Al$_2$O$_3$ (Eq. 2), according to the following reactions [1–6]:

$$3CO + 3H_2 \leftrightarrow CH_3OCH_3 + CO_2 \qquad (1)$$

$$2CH_3OH \leftrightarrow CH_3OCH_3 + H_2O \qquad (2)$$
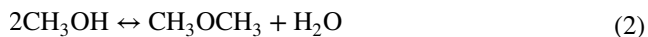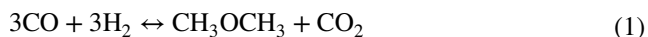
The synthesis of efficient and commercially attractive, robust catalysts has become increasingly challenging due to the both increased demand for DME production and the catalytic process required for methanol to DME process (MTD). Alumina is a cost-efficient material that can be tailored to unique textural properties including high surface area and high porosity. Moreover, alumina can be used as a catalyst support in different oxidation reactions [7, 8]. Therefore, optimizing Al$_2$O$_3$ as a catalyst or a support for such processes remains a topic of great importance [9]. Extensive studies were performed on γ-Al$_2$O$_3$ for MTD reaction. In our previous publication [10]; we showed that γ-Al$_2$O$_3$ and η-Al$_2$O$_3$ catalysts can be prepared from different precursors of aluminium chloride and nitrates, respectively. The produced catalysts showed different surface morphology and acidity with η-Al$_2$O$_3$ showed similar surface characteristics of the commercial zeolite [HZSM-5(80)]. Moreover, η-Al$_2$O$_3$ showed higher catalytic activity during the MTD process than that of the commercial zeolite at reaction temperatures above 275 °C. Thus, η-Al$_2$O$_3$ is considered as a promising catalyst for the commercial production of DME from methanol. Accordingly, kinetic investigation of η-Al$_2$O$_3$ catalyst for the MTD process is needed. To the extent of the authors' knowledge, there has been no detailed kinetic study of η-Al$_2$O$_3$ in MTD reaction along with studying the surface hydrophilicity and acidity, therefore, this area requires further examination.

The dehydration reaction occurs over a solid acid catalyst where its acidity plays a big role in the product distribution. Over very strong acidic sites, further dehydration will take place producing olefins. In order to suppress the dehydration to olefins reaction and increase the selectivity towards the DME, weak or moderate acidity catalysts are desirable as in the Al$_2$O$_3$. Methanol dehydration is known to take place on Lewis acid-pair sites and its rate increases as the surface Lewis acidity increases [11]. It was well reported that γ-Al$_2$O$_3$, a typical Lewis acid catalyst and also the η-Al$_2$O$_3$ used in the study, can catalyse dehydration of MTD [10]. Several reaction mechanisms have been presented for methanol dehydration on acid catalysts [11, 12]. Either Brønsted acid sites or Lewis acid–base pair sites are believed to play a role in such reaction and, generally, the stronger the acid sites the more active the catalysts, however, it should be remembered that as far as Brønsted sites are concerned, their

strength and the reaction temperature should be controlled to avoid hydrocarbons formations [10]. The mechanism based on the Lewis acidity, on the other hand, requires adjacent acid–base pair sites to provide the reaction between the adsorbed alcohol molecule on an acidic site and an adsorbed alkoxide anion on a basic site [11].

The above discussion highlights the importance of studying the reaction kinetics of methanol dehydration over η-Al$_2$O$_3$ catalyst along with studying the different kinetic parameters. Herein, we studied the effect of different operating conditions such as the effect of catalyst weight, % methanol concentration and % water in the reaction feed along the fitted kinetic modelling and correlate the results with the surface hydrophilicity and morphology of η-Al$_2$O$_3$ during the MTD reaction.

2 Experimental

2.1 Materials and Methods

The chemicals used in the present study were all of analytical grade and supplied by Aldrich, UK. The chemicals included aluminium nitrate nonahydrate [Al(NO$_3$)$_3$·9H$_2$O] and ammonia solution (35%). The He and air gases were purchased from BOC with purity 99.99%.

2.2 Catalyst Preparation

The preparation of alumina has been described elsewhere [10]. It was prepared from aluminium nitrate nonahydrate that was then precipitated by ammonia solution giving a precipitate which dried at 120 °C and designated as AN120, followed by calcination at 550 °C and designated as η-Al$_2$O$_3$.

2.3 Catalyst Characterisation

Powder X-ray diffraction (XRD) was carried out using a PANalytical X'Pert Pro X-ray diffractometer. This diffractometer was equipped with a Cu K$_\alpha$ X-ray source with a wavelength of 1.5405 Å. The diffractograms were collected up to 2θ = 80°. The X-ray tube was set at 40 kV and 40 mA. Peaks were selected and compared to diffraction patterns in the software library.

Brunauer–Emmett–Teller (BET) analysis was performed using a Micromeritics ASAP 2020 system. BET surface area and pore volume were measured by N$_2$ adsorption and desorption isotherms at liquid nitrogen temperature (− 196 °C).

TPD-pyridine was used to determine the total surface acidity of the catalyst using the adsorption of pyridine as a probe molecule. Small portions (50 mg) of each sample were preheated to 250 °C for 2 h in the air before exposure to the probe molecule (pyridine) in a sealed desiccator for 2 weeks. The

pyridine-covered samples were subjected to thermogravimetric or differential scanning calorimetry (DSC) analyses on heating up to 600 °C at a heating rate of 10°C min^{-1} in dry N_2 (flow rate = 40 ml min$^-$). The weight loss due to desorption of pyridine from the acidic sites was determined as a function of total surface acidity as sites g_{cat}^{-1} [10].

Scanning electron microscopy (SEM) was carried out on a FEI Quanta 250 FEG MKII with a high-resolution environmental microscope (ESEM) using XT Microscope Control software and linked to an EDX detector. The EDX used was a 10 mm^2 SDD Detector-x-act from Oxford Instruments which utilizes Aztec® EDS analysis software. Both systems used the same chamber.

The static contact angle (CA) of the catalyst pellets with water was measured in order to determine the hydrophilicity of the alumina using a CA meter equipped with a CCD camera (FTA1000 Drop Shape Instrument-B Frame system).

2.4 Catalyst Activity

Catalyst activity tests were conducted in an isothermal fixed-bed reactor made of stainless steel (6 mm OD). The catalyst bed consisted of 50–200 mg (250–425 μm) of a catalyst placed between two plugs of quartz wool. Aera mass flow controllers were used to control the flow of gases to the reactor. The liquid methanol and/or water were injected via a Cheminert® M Series liquid handling pump. A stable flow of methanol vapour to the reactor was established by passing the combined flow of He and methanol through a saturator system, with the evaporation chamber maintained at 150 °C. To prevent condensation, all lines were heated to ~ 150 °C. This mixture was then fed to the fixed bed reactor. The reaction conditions used were different % MeOH in the kinetic experiments under atmospheric pressure over a temperature range from 180 to 350 °C. The total flow rate was 100 cm^3 min^{-1}. Before the reaction, the catalyst was activated in a stream of pure He at 325 °C for 0.5 h under atmospheric pressure stream at a total flow rate of 50 cm^3 min^{-1}. Then, the methanol and He mixture were fed to the reactor and samples analysed by on-line gas chromatography (Perkin-Elmer 500) equipped with a thermal conductivity detector and a flame ionisation detector. A Hayesep DB column was used for the separation of CO, CO$_2$, DME, MeOH, CH$_4$, C$_2$H$_4$, C$_2$H$_6$, ethanol, propanol, and butanol. Each data point was repeated five times to determine the reproducibility of the data for the products.

As shown in Eq. 3, the methanol conversion (X_{MeOH}) was calculated on the basis of the molar flow rate of methanol in the feed ($F_{MeOH,in}$) and in the outlet stream ($F_{MeOH,out}$):

$$X_{MeOH} = \frac{F_{MeOH,in} - F_{MeOH,out}}{F_{MeOH,in}}. \tag{3}$$

DME formation rate (r_{DME}) was determined using Eq. 4, which represents the actual moles of the product, DME, that are present in the reactor outlet stream per gram of the catalyst:

$$r_{DME} = \frac{F_{DME,actual}}{\text{wt. of the catalyst}} \times 100\%. \tag{4}$$

The selectivity for DME (S_{DME}) was determined using Eq. 5 as the ratio (expressed in mol%) between the content of carbon in the product DME and the sum of carbon content corresponding to all observed organic products which are present in the reactor outlet stream:

$$S_{DME} = \frac{2F_{DME}}{F_{CO_2} + F_{CO} + 2F_{DME} + \sum_i n_{Ci}F_i} \times 100\%. \tag{5}$$

Here, F_{DME}, F_{CO_2} and F_{CO} are the molar flow rates of DME, CO$_2$ and CO, respectively in the outlet stream, n_{Ci} is the number of carbon atoms for each of the hydrocarbons (byproducts) and F_i is the molar flow rate of these hydrocarbons [13].

# 3 Results and Discussion

3.1 Catalyst Characterisation

Figure 1 shows the XRD diffractograms of Al(NO$_3$)$_3$·9H$_2$O (precursor), AN120 (as-dried precipitate) and η-Al$_2$O$_3$. The precipitation of aluminium nitrate nonahydrate produced AN120 which showed a mixture of diffractograms of Bayerite (JCPDS 20-11) and Gibbsite (JCPDS 33-18) as shown in diffractograms (b). Interestingly, among all Al(OH)$_3$ structures, Bayerite has the highest symmetry and thermodynamically is the most stable phase and characterised by its crystalline phase [14, 15]. η-Al$_2$O$_3$ diffraction lines (JCDD 04-0875) are shown in diffractograms (c) as a result of the thermal decomposition of Bayerite and Gibbsite at 550 °C.

The pyridine-DSC analysis was used to investigate the surface acidity of the η-Al$_2$O$_3$ catalyst as shown in Fig. 2a which showed mainly two endothermic peaks. The first broad endothermic peak at 80 °C is attributed to the removal of physisorbed water and pyridine along with pyridine desorption from the weak Lewis acidic sites. The small sharp endothermic peak at 235 °C is characterised to the removal of pyridine from moderate Lewis acidic sites [16]. Alumina catalyst, in general, is characterised by its weak acidic sites. From a previous work, η-Al$_2$O$_3$ catalyst showed mainly Lewis acidic sites, thus the DSC results confirmed the presence of weak and medium Lewis acidic sites over the surface of η-Al$_2$O$_3$ catalyst [10].

Fig. 1 XRD patterns of *a* aluminium nitrate nonahydrate, the precursor used in the catalyst preparation, *b* as-dried precipitated at 120 °C (AN120) and *c* η-Al₂O₃ calcined at 550 °C
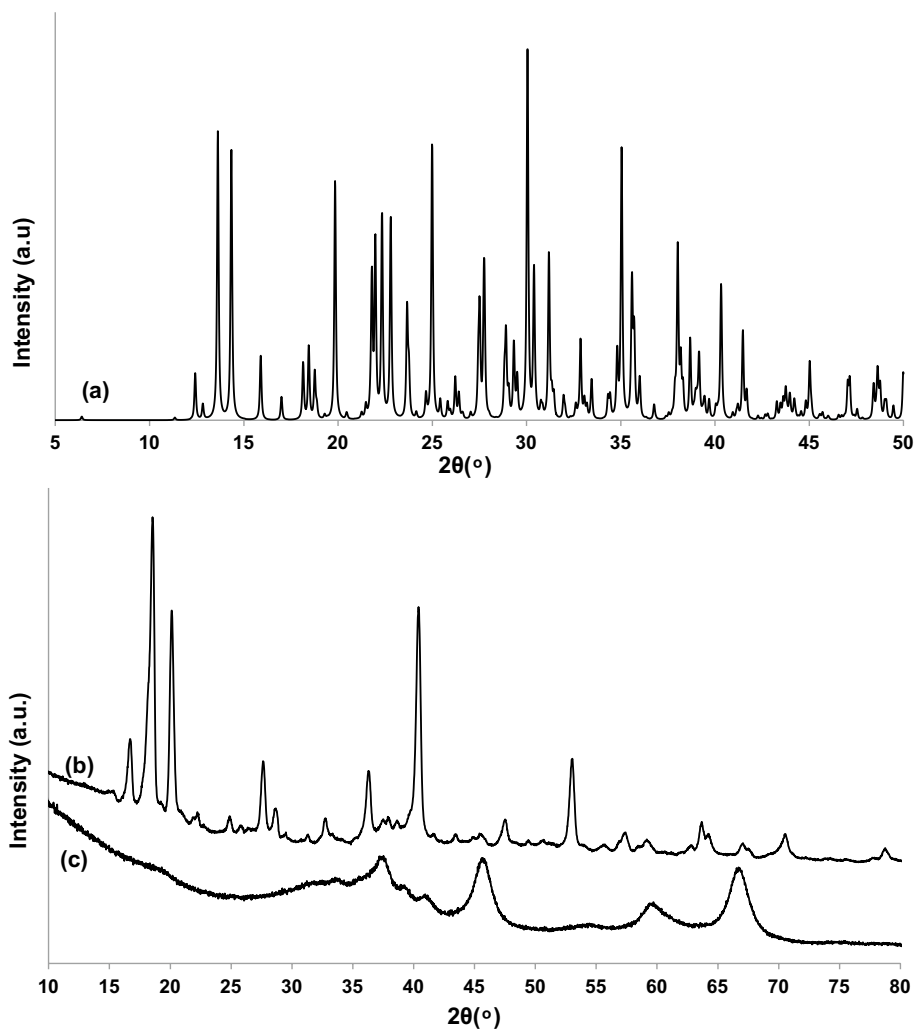
Fig. 2 **a** DSC curve of pyridine–η-Al₂O₃ desorption under N₂ atmosphere with a flow of 40 ml min⁻¹ and heating rate of 10 °C min⁻¹ and **b** the contact water angle of η-Al₂O₃
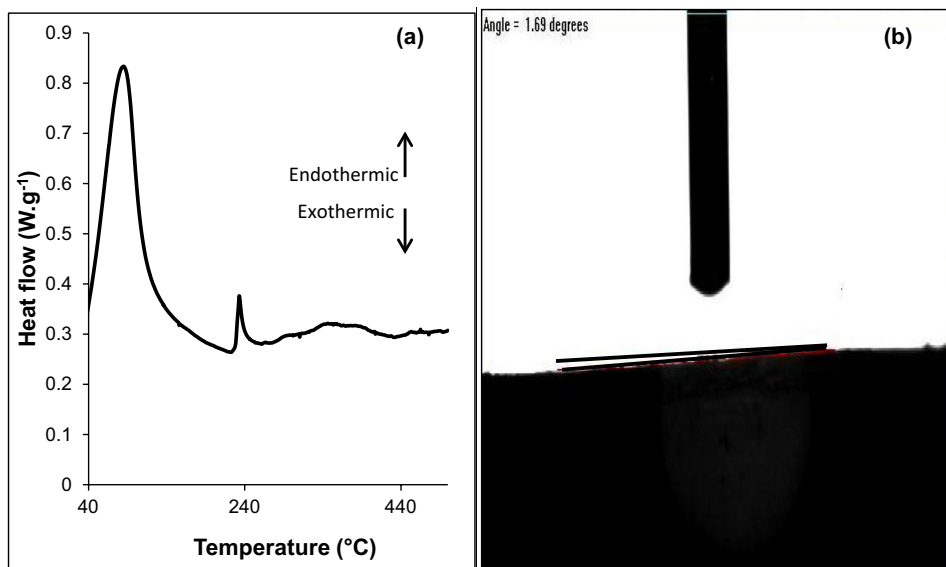
The surface hydrophilicity was determined according to the water CA as seen in Fig. 2b. The wettability of the catalyst surface, demonstrated by CA (θ) of a droplet of water, is assumed by Young's equation (Eq. 6)

$$\cos\theta = \frac{\gamma_{SV} - \gamma_{SL}}{\gamma_{LV}}, \tag{6}$$

where γ_{SV}, γ_{SL} and γ_{LV} stand for the interfacial surface tension of solid (S), liquid (L) and gas vapour (V). This equation is derived from the thermodynamic equilibrium of the free energy at the S–L–V interphase. The surface wettability is measured according to the CA and may be divided into four different categories; super-hydrophilic ($\theta < 10°$), hydrophilic ($10 < \theta < 90°$), hydrophobic ($90 < \theta < 150°$) and super-hydrophobic ($\theta > 150°$). It is well known that pure alumina in general and η-Al_2O_3 specifically is super-hydrophilic with CA approximately $\theta = 1.7°$ as seen in Fig. 2b.

The surface morphology of η-Al_2O_3 was investigated using SEM technique which showed a smaller particle size distribution as shown in Fig. 3. XRD analysis calculation using Scherrer equation showed a crystallite size of 5.5 nm as shown in Table S1. The nitrogen adsorption–desorption isotherms of η-Al_2O_3 catalyst showed type IV isotherm of mesoporous structures as shown in Fig. S1 with a surface area of 223 m^2 g^{-1}.

3.2 Kinetic Study of Pure Alumina

3.2.1 Effect of Different Kinetic Parameters

3.2.1.1 Effect of Catalyst Weight The % methanol conversion was significantly increased with increasing the catalyst weight as seen in Fig. 4. In general, by increasing the catalyst weight from 50 to 200 mg at reaction temperature of
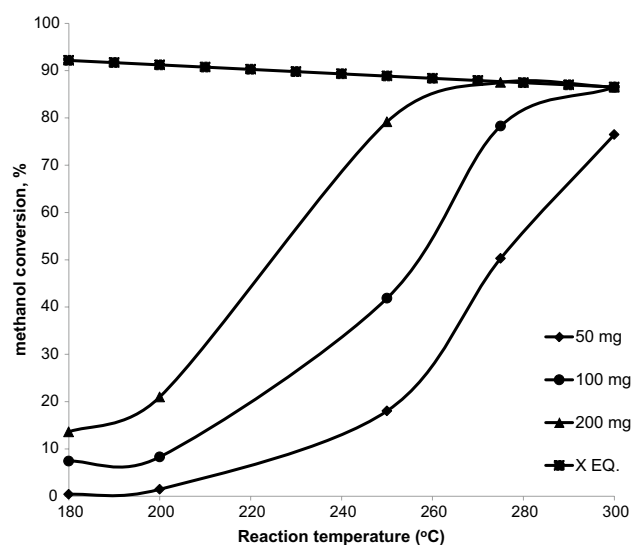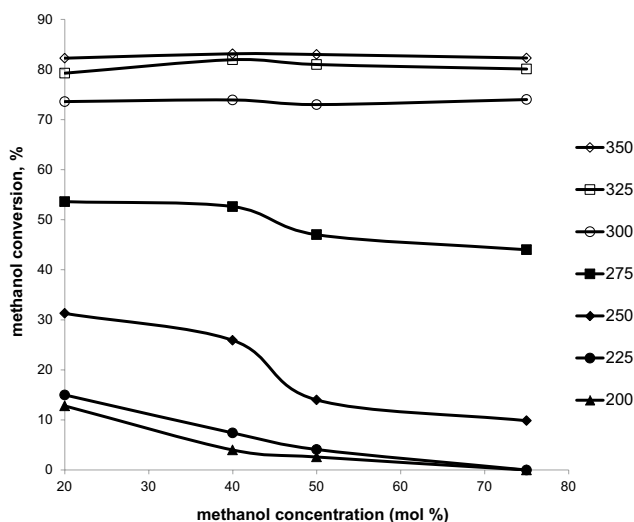
Fig. 4 Effect of catalyst weight on methanol dehydration to DME over η-Al_2O_3 catalysts (T = 180–300 °C, catalyst weight = 50–200 mg, He flow rate = 80 ml min^{-1}, WHSV 12.1 h^{-1}) along with the theoretical equilibrium data (X EQ)

250 °C, the % methanol conversion increased four times. It is apparent that with low catalyst weight in the reactor, i.e., 50 mg, it was insufficient catalyst to facilitate the dehydration reaction below 200 °C with $T_{50\%}$ of 275 °C. However, by increasing the catalyst weight to 200 mg, an increase in methanol conversion was observed as there are more active acidic sites species present to facilitate the MTD reaction with $T_{50\%}$ of 222 °C.

3.2.1.2 Effect of Methanol Concentration Figure 5 clearly shows that, in general, the % methanol conversion is inversely proportional to the % concentration of methanol
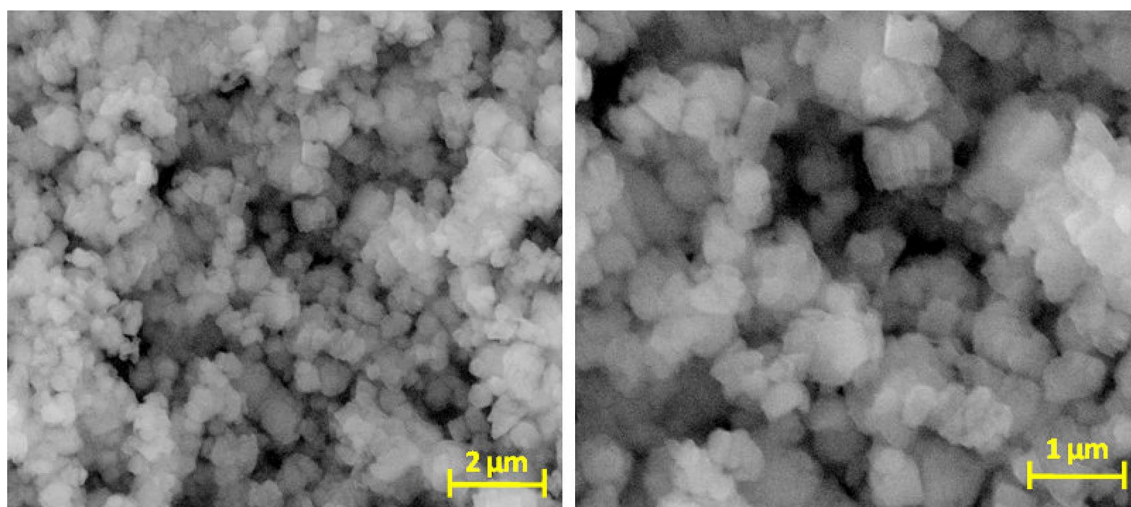
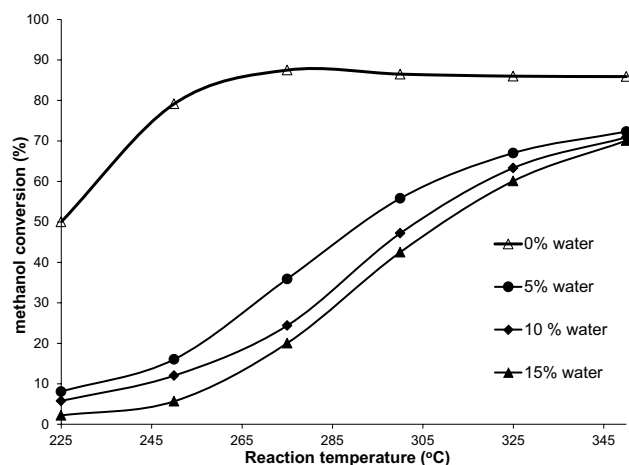**Fig. 3** SEM images of η-Al_2O_3 catalysts at different levels of magnifications using the ETD detector

Fig. 5 Effect of methanol concentration in the reaction feed of methanol dehydration to DME reaction over η-Al$_2$O$_3$ catalysts, (T = 200–350 °C, catalyst weight = 200 mg, He flow rate = 80 ml min^{-1}, WHSV 12.1 h^{-1})

Fig. 6 Effect of water in the reaction feed of methanol dehydration to DME reaction over η-Al$_2$O$_3$ catalysts (T = 225–350 °C, catalyst weight = 200 mg, He flow rate = 80 ml min^{-1}, WHSV 12.1 h^{-1})

in the reaction feed. The inhibition effect is minor at reaction temperature above 300 °C. In contrast, the inhibition effect of methanol concentrations at reaction temperature below 275 °C is obvious; for instance, at reaction temperature of 250 °C, the % conversion decreased by 20% upon increasing the % methanol concentration from 20 to 75% in the reaction feed. This inhibition effect is due to the crowded alcohol molecules, over the surface active sites, which retard the dehydration of CH$_3$OH to produce DME. This is, consequently, reflected on the values of % conversion, where its values gradually reduced with increasing the alcohol concentration in the reaction feed.

3.2.1.3 Effect of Water in the Feed Figure 6 shows the inhibition effect of water on the MTD process. During the methanol dehydration reaction, water is produced which also has a significant effect on catalyst deactivation [17–20] as η-Al$_2$O$_3$ is super-hydrophilic [21], and facilitates strong water adsorption. Both water and methanol compete for adsorbing on the active sites of η-Al$_2$O$_3$ with water being adsorbed more strongly [17]. Osman et al. [5] showed that is possible to increase the hydrophobicity of the support thereby reducing the deactivation by water. The catalytic activity dramatically decreased by five times upon adding of 5% water in the reaction feed at a reaction temperature of 250 °C and then slightly decreased by adding further water in the reaction feed (15%). The water inhibition effect is insignificant at a reaction temperature above 300 °C as the water adsorption on the active alumina site is not that strong.

Development of new and cheap catalysts for MTD process on a large scale is of great interest. Usually, methanol

is converted over solid catalyst either as simply dehydration, yielding DME and water, or as deep dehydration, producing hydrocarbons [22]. At the reaction conditions used [240–300 °C]; hydrocarbons products were hardly detected as a side reaction product [10]. The kinetics of methanol dehydration on acidic catalysts has been studied extensively resulting in different kinetics equations. A list of kinetic models for MTD is given in Table 1 [23].

It is evident that some of the rate equations for dehydration where the reaction rate are proportional to the square root of the methanol concentration. This indicates that the MTD reaction undergoes dissociative adsorption of methanol on the catalyst surface [27].

It is stated in Froment and Bischoff [30] that the reaction rate for surface catalysed reactions with a mechanism is based on chemisorption and a single rate-determining step, which can be written as a combination of three groups. These are a kinetic group, a driving-force group, and an adsorption group. The rate is thus expressed as

$$-r_{\text{MeOH}} = \frac{\text{(kinetic factor)(driving force group)}}{\text{(adsorption group)}^n} = \frac{K\Phi(P, Y_j^0, X_{CO}K_P)}{\Phi(P, Y_j^0, X_{CO}K_{J,a})},$$ (7)

where kinetic factor = k, the Arrhenius equation is used to describe the variation of the rate constant with temperature

$$k = k_0 \exp(-E_a/RT),$$ (8)

driving force group = $\Phi\left(P, y_j^0, X_{CO}, K_P\right)$

K_P is the equilibrium constant for MTD reaction (Eq. 2):

$$\log K_P = \frac{4019}{T} + 3.707 \log T - 2.783 \times 10^{-3} T$$
$$+ 3.8 \times 10^{-7}T^2 - 6.56 \times 10^4 T^3 - 26.64,$$ (9)

Table 1 Reaction kinetic equation for various acidic catalysts used for MTD reaction

No.	Reaction kinetic equation[a]	Catalyst used	References
1	$-r_M = \dfrac{k_1 P_M^{1/2}}{P_M^{1/2} + k_2 P_w}$	Al_2O_3	Kallo and Knozinger [24]
2	$-r_M = \dfrac{k K_M P_M^{1/2}}{1 + K_M P_M^{1/2} + K_w P_w}$	Al_2O_3	Figueras et al. [25]
3	$-r_M = \dfrac{k K_M^2 \left[P_M^2 - \left(\frac{P_W P_D}{K_{eq}} \right) \right]}{\left[1 + 2(K_M P_M)^{1/2} + K_W P_W \right]^4}$	Acidic ion exchange resin	Klusacek and Schneider [26]
4	$r_{DME} = \dfrac{k K_M^2 \left[P_M^2 - \left(\frac{P_W P_D}{K_{eq}} \right) \right]}{\left[1 + 2(K_M P_W)^{\frac{1}{2}} + K_W P_W \right]^4}$	γ-Al_2O_3	Bercic and Levec [27]
5	$r_{DME} = \dfrac{k K_M P_M^{1/2}}{1 + K_M P_M^{1/2} K_W P_W}$	γ-Al_2O_3	Bercic and Levec [27]
6	$-r_M = \dfrac{k \left[\frac{P_M^2}{P_W} - \left(\frac{P_D}{K_{eq}} \right) \right]}{(1 + K_M P_M + K_W P_W)^2}$	HZSM-5	Lu et al. [28]
7	$-r_M = \dfrac{k P_M \left[1 - \left(\frac{P_D P_W}{K_{eq} P_M^2} \right) \right]}{1 + K_M P_M + P_W / K_W}$	γ-Al_2O_3	Mollavali et al. [29]

[a]k: kinetic factor

$r_{(M \text{ or } D)}$ is the reaction rate for the species where M or D is methanol or dimethyl ether, respectively

$P_{(M,W \text{ or } D)}$ is the partial pressure for the species where M,W or D is methanol, water or dimethyl ether, respectively

$K_{(M,W \text{ or } D)}$ is the adsorption equilibrium constant where M,W or D is methanol, water or dimethyl ether, respectively

(adsorption group)$^n = \Phi\left(P, y_j^0, X_{CO}, K_{j,a} \right)^n$, where $K_{j,a}$ is the adsorption equilibrium constants defined by the van't Hoff equation

$$K_{j,a} = A_j \exp\left(-\Delta H_{j,a}^0 / RT \right). \tag{10}$$

The kinetic data were obtained in an integral reactor where the methanol conversions greater than 10% are produced. For an integral plug-flow reactor, the reaction rate is calculated as:

$$-r_{MeOH} = \frac{dX_{MeOH}}{d(E/F_{MeOH}^0)}. \tag{11}$$

The integration of the rate equation over the reactor bed leads to:

$$\frac{W}{F_{MeOH}^0} = f(X_{MeOH}, k, K_j \ldots). \tag{12}$$

Here, the methanol conversion for Eq. 12 was performed by applying numerical integration using fourth order Runge–Kutta method, the MATLAB subroutine function ODE15s.

The parameter estimation was based on minimization of the objective function using the sum of residual squares:

$$\sum_{i=1}^{n} \left(X_{MeOH} - \hat{X}_{MeOH} \right)^2, \tag{13}$$

where n is the total number of experiments, X is the experimental methanol conversion, and $\hat{X}$ is the calculated methanol conversion.

3.2.2 Validation of the Kinetic Model

To determine the validity of the model, we applied F test (Eq. 14) and R^2 a coefficient of determination (Eq. 15). It is stated that if $R^2 > 0.9$ and $F > 10 \times F_{0.05}$, we can say that the model is reliable.

$$F_c = \frac{\sum_{i=1}^{n} \frac{\hat{X}_{MeOH}^2}{p}}{\sum_{i=1}^{n} \frac{(X_{MeOH} - \hat{X}_{MeOH})^2}{n-p}} ? \gtrless F(p, n-p; 1-\alpha), \tag{14}$$

where n is number of the experiments, p a is number of parameters in the equation of model, and $1 - \alpha$ is the confidence level. If the calculated F value is higher than the tabulated ones, the regression is statistically meaningful.

The highest calculated F value corresponds to the model that best fits the experimental data.

$$R^2 = 1 - \frac{\sum_{i=1}^{n} (X_{\text{MeOH}} - \hat{X}_{\text{MeOH}})^2}{\sum_{i=1}^{n} X_{\text{MeOH}}^2}. \tag{15}$$

Statics results and values of activation energy and heat of adsorption of methanol and water for the fitted proposed models are tabulated in Table 2. It is clear that from the statistics values that the best model to fit the experimental data is Bercic model that the dehydration reaction undergoes dissociative adsorption Langmuir–Hinshelwood mechanism of methanol on the catalyst surface. The calculated value of the activation energy is 136.7 kJ mol⁻¹ which is in agreement with the one estimated by Bercic and Levec [27] (143.7 kJ mol⁻¹). For the heat of adsorption of methanol and water are 68.7 and 44.3 kJ mol⁻¹, respectively, which are comparable with the values by Bercic and Levec [27] 70.5 and 41.1, respectively. Lu et al. [28] developed a detailed intrinsic mechanism containing seven elementary reactions, where Mollavali et al. [29] used Lu's mechanism with different limiting step to derive kinetic global reaction equation.

The above values of heat of adsorption of water and methanol confirm that the inhibition effect of water is greater than that of methanol. For instance, at a reaction temperature of 250 °C, when water introduced in the reaction feed to the value of 5%, the % methanol conversion dramatically decreased by 63% from the initial conversion of the dry feed as seen in Fig. 6. On the other hand, by doubling the methanol concentration in the reaction feed from 20 to 40%, the methanol conversion slightly decreased by 5.4% as seen in Fig. 5. Moreover, the inhibition effect for both water and methanol decreased with increasing the reaction temperature, for instance in the case of water when the reaction temperature increased from 250 to 350 °C for 5% water in the feed, the % methanol conversion increased from 16 to 72%, respectively. In other words, at a reaction temperature of 350 °C, the % conversion of methanol for 5% water in the feed decreased by only 15% from the initial conversion of the dry feed. This can be explained by Eq. 10, as the reaction temperature increased, the desorption equilibrium value of water increased which means that water will be easily desorbed from the surface of the alumina catalyst at high reaction temperature, thus the inhibition effect of either

water or methanol will be of minor significance at high reaction temperature. The fitted kinetic modelling results are in agreement with the surface morphology of η-Al₂O₃ which explained the strong water inhabitation effect that comes from the super-hydrophilicity nature of η-Al₂O₃ with CA approximately θ = 1.7° as seen in Fig. 2b which is in agreement with the kinetic model shown in Table 2. Moreover, during the reaction mechanism, water is produced which has a significant effect on the alumina catalyst deactivation, as water and methanol compete for adsorbing on the active sites of alumina catalyst with water being adsorbed more strongly [31]. It is worth noting that in our previous publication we showed that the prepared η-Al₂O₃ has similar morphology and surface acidity of zeolite [HZSM-5(80)] which is in line with the fitted kinetic modelling as our work matched with Lu model who studied the kinetic modelling of zeolite as shown in Table 2 [10].

The simulation and experimental results are given in the parity plot of Fig. 7, which compares the experimental conversions of methanol with those predicted by solving Bercic model and revealed that from the statistics values
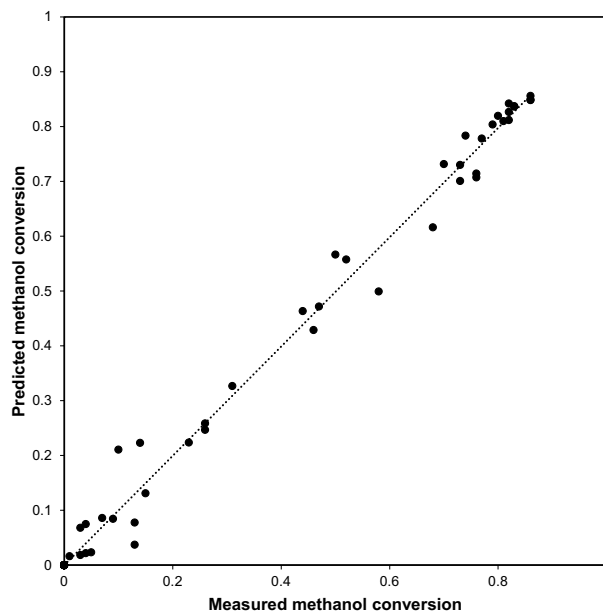

Fig. 7 Comparison of measured and predicted MeOH Conversion for Bercic equation model

Table 2 Statics results and values of activation energy and heat of adsorption of methanol and water for the proposed model

Refs.	n	n−p	F	10 × F₀.₀₅	R²	Eₐ	H_MeOH	H_H₂O
Bercic and Levec [27]	36	30	1075	24.2	0.9954	136.7	68.7	44.3
Mollavali et al. [29]	36	30	416.3	24.2	0.9873	135.8	47.8	65.1
Lu et al. [28]	36	30	518	24.2	0.9903	137.2	63.9	59.3

that the best model to fit the experimental data was Bercic model.

4 Conclusions

Kinetic modeling studies were used to investigate the reaction mechanism of methanol dehydration over the pure η-Al$_2$O$_3$ catalyst and revealed that from the statistics values that the best model to fit the experimental data was Bercic model which was in agreement with literature that the dehydration reaction undergoes dissociative adsorption Langmuir–Hinshelwood mechanism of methanol on the catalyst surface. The calculated value of the activation energy is 136.7 kJ mol^{-1}, where, the heat of adsorption of methanol and water are 68.7 and 44.3 kJ mol^{-1}, respectively. The % methanol conversion was significantly increased with increasing the catalyst weight, while it was dramatically decreased with increasing either the % methanol or water in the reaction feed at the low reaction temperature (<250 °C).

References

1. Khoshbin R, Haghighi M (2014) Direct conversion of syngas to dimethyl ether as a green fuel over ultrasound-assisted synthesized CuO–ZnO–Al$_2$O$_3$/HZSM-5 nanocatalyst: effect of active phase ratio on physicochemical and catalytic properties at different process conditions. Catal Sci Technol 4(6):1779–1792

2. Figoli NS, Hillar SA, Parera JM (1971) Poisoning and nature of alumina surface in the dehydration of methanol. J Catal 20(2):230–237

3. Asthana S, Samanta C, Bhaumik A, Banerjee B, Voolapalli RK, Saha B (2016) Direct synthesis of dimethyl ether from syngas over Cu-based catalysts: enhanced selectivity in the presence of MgO. J Catal 334:89–101

4. Cai M, Palčić A, Subramanian V, Moldovan S, Ersen O, Valtchev V et al (2016) Direct dimethyl ether synthesis from syngas on copper–zeolite hybrid catalysts with a wide range of zeolite particle sizes. J Catal 338:227–238

5. Osman AI, Abu-Dahrieh JK, McLaren M, Laffir F, Nockemann P, Rooney D (2017) A facile green synthetic route for the preparation of highly active γ-Al$_2$O$_3$ from aluminum foil waste. Sci Rep 7(1):3593

6. Osman AI, Abu-Dahrieh JK, Abdelkader A, Hassan NM, Laffir F, McLaren M et al (2017) Silver-modified η-Al$_2$O$_3$ catalyst for DME production. J Phys Chem C 121(45):25018–25032

7. Osman AI, Meudal J, Laffir F, Thompson J, Rooney D (2017) Enhanced catalytic activity of Ni on η-Al$_2$O$_3$ and ZSM-5 on addition of ceria zirconia for the partial oxidation of methane. Appl Catal B 212:68–79

8. Osman AI, Abu-Dahrieh JK, Laffir F, Curtin T, Thompson JM, Rooney DW (2016) A bimetallic catalyst on a dual component support for low temperature total methane oxidation. Appl Catal B 187:408–418

9. Royaee SJ, Falamaki C, Sohrabi M, Talesh ASS (2008) A new Langmuir–Hinshelwood mechanism for the methanol to dimethylether dehydration reaction over clinoptilolite–zeolite catalyst. Appl Catal A 338(1–2):114–120

10. Osman AI, Abu-Dahrieh JK, Rooney DW, Halawy SA, Mohamed MA, Abdelkader A (2012) Effect of precursor on the performance of alumina for the dehydration of methanol to dimethyl ether. Appl Catal B 127:307–315

11. Hosseininejad S, Afacan A, Hayes RE (2012) Catalytic and kinetic study of methanol dehydration to dimethyl ether. Chem Eng Res Des 90(6):825–833

12. Akarmazyan SS, Panagiotopoulou P, Kambolis A, Papadopoulou C, Kondarides DI (2014) Methanol dehydration to dimethylether over Al$_2$O$_3$ catalysts. Appl Catal B 145:136–148

13. Abu-Dahrieh J, Rooney D, Goguet A, Saih Y (2012) Activity and deactivation studies for direct dimethyl ether synthesis using CuO–ZnO–Al$_2$O$_3$ with NH$_4$ZSM-5, HZSM-5 or γ-Al$_2$O$_3$. Chem Eng J 203(0):201–211

14. Jiao WQ, Yue MB, Wang YM, He MY (2012) Synthesis of morphology-controlled mesoporous transition aluminas derived from the decomposition of alumina hydrates. Microporous Mesoporous Mater 147(1):167–177

15. Wefers K, Misra C (1987) Oxides and hydroxides of aluminum. Alcoa Technical Paper No. 19, revised

16. Dumitriu E, Hulea V (2003) Effects of channel structures and acid properties of large-pore zeolites in the liquid-phase tert-butylation of phenol. J Catal 218(2):249–257

17. Alamolhoda S, Kazemeini M, Zaherian A, Zakerinasab MR (2012) Reaction kinetics determination and neural networks modeling of methanol dehydration over nano γ-Al$_2$O$_3$ catalyst. J Ind Eng Chem 18:2059–2068

18. Xu M, Lunsford JH, Goodman DW, Bhattacharyya A (1997) Synthesis of dimethyl ether (DME) from methanol over solid-acid catalysts. Appl Catal A 149(2):289–301

19. Lertjiamratn K, Praserthdam P, Arai M, Panpranot J (2010) Modification of acid properties and catalytic properties of AlPO$_4$ by hydrothermal pretreatment for methanol dehydration to dimethyl ether. Appl Catal A 378(1):119–123

20. Raoof F, Taghizadeh M, Eliassi A, Yaripour F (2008) Effects of temperature and feed composition on catalytic dehydration of methanol to dimethyl ether over alumina. Fuel 87(13–14):2967–2971

21. Kim SD, Baek SC, Lee Y-J, Jun K-W, Kim MJ, Yoo IS (2006) Effect of γ-alumina content on catalytic performance of modified ZSM-5 for dehydration of crude methanol to dimethyl ether. Appl Catal A 309(1):139–143

22. Ladera RM, Ojeda M, Fierro JLG, Rojas S (2015) TiO$_2$-supported heteropoly acid catalysts for dehydration of methanol to dimethyl ether: relevance of dispersion and support interaction. Catal Sci Technol 5(1):484–491

23. Zhang L, Zhang H-T, Ying W-Y, Fang D-Y (2011) Intrinsic kinetics of methanol dehydration over Al$_2$O$_3$ catalyst. World Acad Sci Eng Technol 59:1538–1543

24. Kallo D, Knozinger H (1967) Dehydratisierung von alkoholen an aliminiumoksid. Chem Ing Tech 39:676–680

25. Figueras F, Nohl A, Mourgues L, Trambouze Y (1971) Dehydration of methanol and *tert*-butyl alcohol on silica-alumina. Trans Faraday Soc 67:1155–1163

26. Klusacek K, Schneider P (1982) Stationary catalytic kinetics via surface concentrations from transient data methanol dehydration. Chem Eng Sci 37:1523–1528

27. Bercic G, Levec J (1992) Intrinsic and global reaction rate of methanol dehydration over gamma-alumina pellets. Ind Eng Chem Res 31(4):1035–1040

28. Lu W-Z, Teng L-H, Xiao W-D (2004) Simulation and experiment study of dimethyl ether synthesis from syngas in a fluidized-bed reactor. Chem Eng Sci 59(22–23):5455–5464

29. Mollavali M, Yaripour F, Atashi H, Sahebdelfar S (2008) Intrinsic kinetics study of dimethyl ether synthesis from methanol on γ-Al$_2$O$_3$ catalysts. Ind Eng Chem Res 47(9):3265–3273

30. Hofmann H (1991) In: Von Froment GF, Bischoff KB (eds) Chemical reactor analysis and design. Wiley, New York 1990. 2. Aufl., XXXIV, 664 S., zahlr. Abb. u. Tab., Ln. Chem Ing Tech 63(2):103–103

31. Osman AI, Abu-Dahrieh JK, Rooney DW, Thompson J, Halawy SA, Mohamed MA (2017) Surface hydrophobicity and acidity effect on alumina catalyst in catalytic methanol dehydration reaction. J Chem Technol Biotechnol 92(12):2952–2962